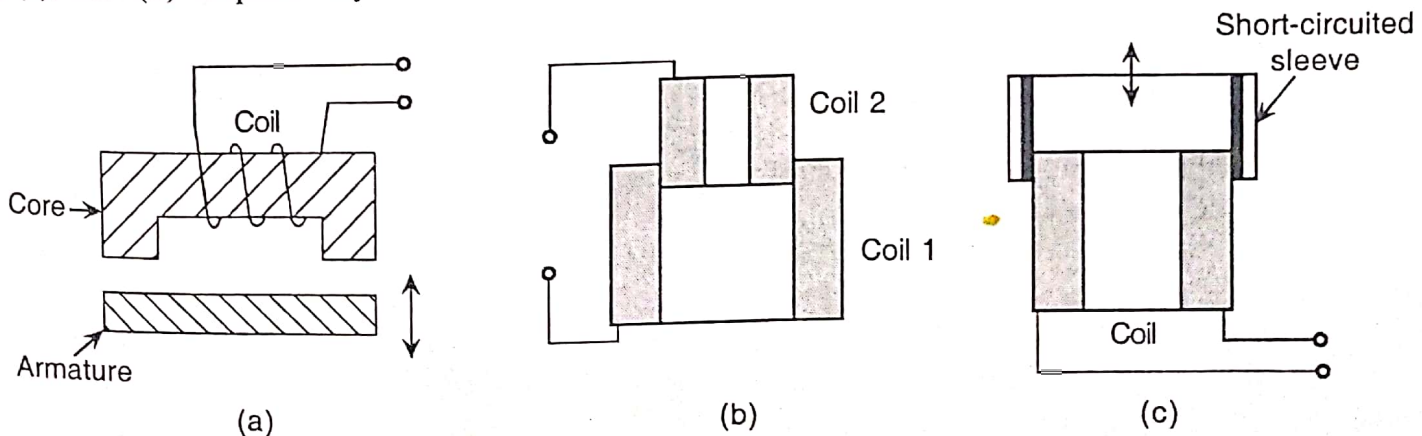


2.4 INDUCTIVE SENSORS

Although specific cases of inductive technique of sensing and/or transducing have been dealt in detail in Chapter 4 on magnetic sensors, a generalized discussion on inductive sensing is given in this section.

The inductive transducer utilizes the simple principle that the physical quantity, such as motion, to be measured can be made to vary the inductance of a coil, maintaining a relation between the two. This variation of inductance can often be measured by ac bridge circuits, or can be made to produce a voltage if it is magnetically coupled to another coil carrying a flux or voltage. If a magnetostrictive core material is used, force or pressure can change the permeability which can be measured as a change in inductance of a coil around the core.

The two most common methods of achieving variation in inductance are (i) by changing the reluctance of the magnetic path and (ii) by coupling two or more elements. The latter technique works by (a) change of mutual inductance, (b) change of eddy current when one element is just a short-circuited sleeve, and (c) transformer action. These are shown schematically in Figs. 2.17(a), (b), (c), and (d) respectively.



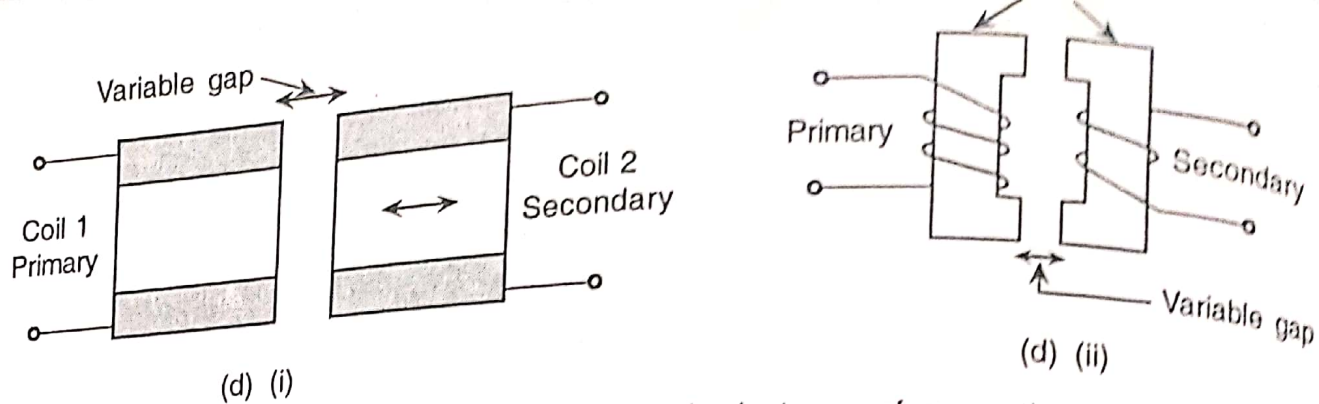


Fig. 2.17 Inductive sensors using (a) change of reluctance of magnetic path, (b) change of mutual inductance between two coils, (c) change of mutual inductance between a coil and a sleeve, and (d) (i) and (ii) transformer action.

Then there are inductive sensors of (i) the electromagnetic type which are bilateral in operation with electrical and mechanical input/output relationship and (ii) the magnetostriictive type. A sensor that uses a magnetostriictive core material is shown in Fig. 2.18.

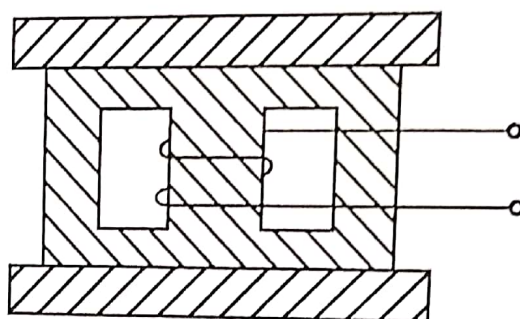


Fig. 2.18 Sensor using a magnetostriictive effect.

Inductance variation can also be achieved by variation of coil geometry such as coil length but such a procedure is not very convenient to be adopted in practice.

It is observed that a coil is an essential part of inductive transducers and the coil may be wound on a metal (iron) core or an air core. In the variable reluctance type, the core is a ferromagnetic material as also the armature. This type of sensors are, perhaps, the most extensively used because it (i) is the most sensitive one, (ii) is least affected by external fields as the air gap is least, and (iii) requires less number of turns than in air core design for same value of inductance so that interwinding or self-capacitance and stray effects are less. The copper coil on a ferromagnetic core has an equivalent circuit that consists of an inductance L in series with copper loss resistance R_c and a resistance R_e , representing eddy loss resistance in the core in parallel with coil resistance R_c and inductance L . The equivalent circuit is shown in Fig. 2.19.

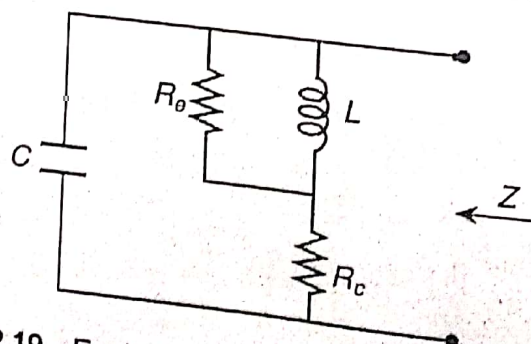


Fig. 2.19 Equivalent circuit of a ferromagnetic coil.

If a coil has n turns, a current I , and the core length l , the field strength H is given by

$$H = \frac{nI}{l} \text{ (A/m)} \quad (2.16)$$

For a core material of permeability μ , which often is expressed as the product of its relative permeability and the permeability of the free space or vacuum ($\mu_0 = 4\pi \times 10^{-7}$ H/m), and core cross-section area a , the self inductance L of the coil is the flux linkage per unit current so that

$$L = \frac{n\phi}{I} = n \frac{Ba}{I} = n \frac{\mu Ha}{I} \quad (2.17)$$

where B is in Tesla or Wb/m² and ϕ is in Wb.

Using Eq. (2.16), one derives

$$L = \frac{\mu n^2 a}{l} \text{ (Henries)} \quad (2.18)$$

The copper resistance R_c is also easily calculated if the coil wire diameter d and the copper resistivity ρ are known, so that

$$R_c = \frac{4\rho nl_t}{\pi d^2} \quad (2.19)$$

where l_t is the average length per turn of the coil. The coil dissipation factor D_c is usually defined as

$$D_c = \frac{R_c}{\omega L} \quad (2.20)$$

which decreases with increasing frequency.

For reducing eddy loss or core loss as it is called (the core is usually made of laminations of certain thickness, say t_l), the depth of penetration of eddy current, d_p is given by

$$d_p = \sqrt{\frac{\rho_e}{\pi \mu f}} \quad (2.21)$$

where ρ_e is the resistivity of the core material and $f = \omega/(2\pi)$ is the frequency. The eddy loss resistance is then given by

$$R_e = \left(\frac{2d_p \omega L}{t_l} \right) \left[\frac{\cosh\left(\frac{t_l}{d_p}\right) - \cos\left(\frac{t_l}{d_p}\right)}{\sinh\left(\frac{t_l}{d_p}\right) - \sin\left(\frac{t_l}{d_p}\right)} \right] \quad (2.22)$$

Equations (2.21) and (2.22) are valid only for low frequencies when $\rho_t = (t_l/d_p) \leq 2$. The frequency range, however, varies depending on the core material as well as lamination thickness. Figure 2.20 shows the plots of f versus t for different materials of commercial importance for $\rho_t \approx 2$, so that within this range of frequency Eq. (2.22) can be simplified using Eqs. (2.18) and (2.21) as

$$R_e \approx \frac{6\omega L}{(t_l/d_p)^2} = \frac{12\rho_e a n^2}{(lt_l)^2} \quad (2.23)$$

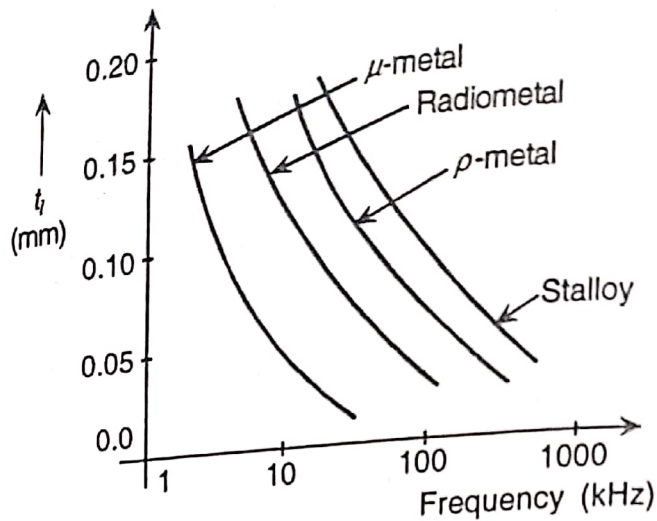


Fig. 2.20 Sheet thickness versus frequency plots for different magnetic materials.

This figure (Fig. 2.20) shows what frequency range can be covered by a specific material with specified thicknesses.

The eddy loss dissipation factor is defined by

$$D_e = \frac{\omega L}{R_e} \quad (2.24)$$

and is directly proportional to frequency.

Magnetic material undergoes hysteresis and this causes dissipation or loss. The area within the hysteresis curve is given by

$$A_h = \int B \cdot dH \quad (2.25)$$

where H is the magnetic field strength and B is the magnetic induction.

The B - H loop for a ferromagnetic material is schematically shown in Fig. 2.21. Following Rayleigh's procedure, the area A_h has been computed and hence, the energy dissipated per unit volume. For a core of cross-sectional area a , and length l , total hysteresis loss, in this way, is obtained as

$$P_h = \left(\frac{16\pi}{3} \right) a \alpha_r H_l^3 f \times 10^{-7} \quad (\text{watts}) \quad (2.26)$$

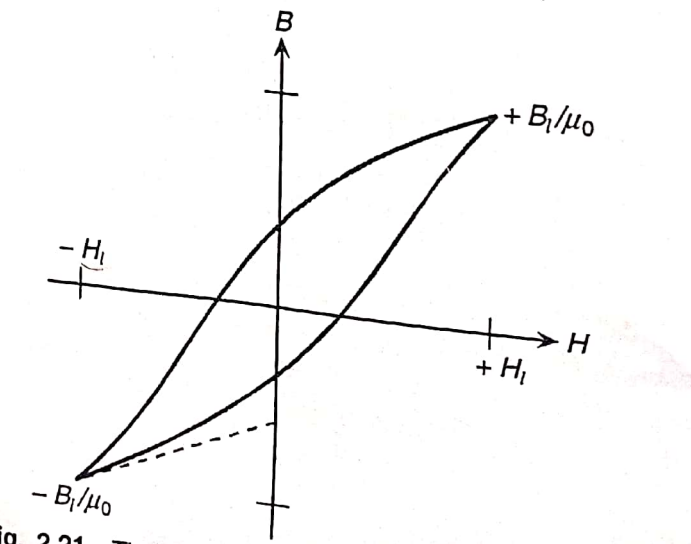


Fig. 2.21 The B - H loop for a magnetic material.

where α_r is the Rayleigh's constant which may be defined by the equation

$$\alpha_r = 2 \frac{\left(\frac{\Delta B}{\mu_0} - \mu_i H \right)}{(\Delta H)^2} \quad (2.27)$$

where μ_i is the initial permeability, that is, permeability at $H = 0$. With change from zero values of B and H , Eq. (2.27) is written as

$$\alpha_r = \frac{2(B/\mu_0 - \mu_i H)}{H^2} \quad (2.28)$$

Using $P_h = E^2/R_h$, R_h , being the equivalent hysteresis loss resistance, is

$$R_h = \frac{\omega^2 L^2 I^2}{P_h} \quad (2.29)$$

which is proportional to the square of the frequency. However, the hysteresis dissipation factor D_h is given by

$$D_h = \frac{\omega L}{R_h} = \frac{2\alpha_r H_l}{(3\pi\mu_i)} \quad (2.30)$$

which is independent of frequency.

A sensor or a transducer involves the movement of an armature, that is, the situation demands that the core has an air gap, the length of which varies with the value of the measured quantity such as a motion. This is taken into consideration by determining the effective permeability of the core when the sample permeability μ_s is known and a relation between L and the gap length l_g can be found. Thus, for a toroidal ring sample of total path length l , gap length l_g , cross-sectional area a , the effective permeability μ , we obtain

$$\frac{\left(\frac{(l - l_g)}{\mu_s} + l_g \right)}{a} = \frac{l}{\mu a} \quad (2.31)$$

yielding

$$\mu = \frac{\mu_s}{\left\{ 1 + \left(\frac{l_g}{l} \right) (\mu_s - 1) \right\}} \quad (2.32a)$$

Since $\mu_s \gg 1$,

$$\mu \approx \frac{\mu_s}{\left\{ 1 + \left(\frac{l_g}{l} \right) \mu_s \right\}} \quad (2.32b)$$

Substituting this in Eq. (2.18),

$$L = \left[\frac{\mu_s}{\left\{ 1 + \left(\frac{l_g}{l} \right) \mu_s \right\}} \right] \left(\frac{n^2 a}{l} \right) \text{ (Henries)} \quad (2.33)$$

Before moving on to the analysis of change of inductance with air gap and its nature, the effect of the capacitor C of Fig. 2.19 is considered. This capacitance arises, as already mentioned, due to the coil self-capacitance, that is, interwinding capacitance as also due to the connecting cable capacitance. The effect of parallel resistance R_e can be considered in series with the inductance so that the total series resistance R , is then used to calculate the impedance Z as

$$Z = \frac{R + j\omega L}{(1 - \omega^2 LC) + j\omega RC} \quad (2.34)$$

which, on rationalization, can be written as

$$Z = \frac{R}{(1 - \omega^2 LC)^2 + (\omega^2 LC/Q)^2} + j\omega L \frac{(1 - \omega^2 LC) - (\omega^2 LC/Q^2)}{(1 - \omega^2 LC)^2 + (\omega^2 LC/Q)^2} \quad (2.35)$$

where $Q = L/R$.

For a good inductor with $Q^2 \gg 1$, we get

$$Z = \frac{R}{(1 - \omega^2 LC)^2} + \frac{j\omega L}{(1 - \omega^2 LC)} = R_{eq} + j\omega L_{eq} \quad (2.36)$$

indicating that both R_{eq} and L_{eq} increase but the effective Q , Q_{eq} decreases

$$Q_{eq} = \frac{\omega L (1 - \omega^2 LC)}{R} \quad (2.37)$$

2.4.1 Sensitivity and Linearity of the Sensor

For a small air gap l_g and effective permeability of the core μ , the inductance is given by Eq. (2.33). Now since n and a are constants, using

$$K_l = 4\pi \times 10^{-7} n^2 a \quad (2.38)$$

Equation (2.33) can be written as

$$L = \frac{K_l}{\left(l_g + \frac{l}{\mu_s}\right)} \quad (2.39)$$

from which assuming $l \gg l_g$, for small increase or decrease in gap l_g and ∂l_g ,

$$\begin{aligned} \frac{\partial L}{L} &= \frac{\partial l_g}{\left(l_g \pm \frac{\partial l_g}{\mu_s} + \frac{l}{\mu_s}\right)} \\ &= \frac{\partial l_g/l_g}{1 + \frac{l}{l_g \mu_s}} \cdot \frac{1}{1 \pm \frac{(\partial l_g/l_g)}{\{1 + l/(l_g \mu_s)\}}} \end{aligned} \quad (2.40a)$$

and for $(\partial l_g/l_g)/(1 + l/(l_g \mu_s)) \ll 1$.

$$\frac{\partial L}{L} = \frac{\partial l_g/l_g}{1 + \frac{l}{l_g \mu_s}} \left[1 \mp \frac{\partial l_g/l_g}{1 + \frac{l}{l_g \mu_s}} + \left(\frac{\partial l_g/l_g}{1 + \frac{l}{l_g \mu_s}} \right)^2 \mp \dots \right] \quad (2.40b)$$

If only the first term is accepted for ∂l_g being very small, there appears to be a linear variation between L and l_g , and the sensitivity $S_{l_g}^L = (\partial L/L)/(\partial l_g/l_g)$ is given as

$$S_{l_g}^L = \frac{1}{1 + l/(l_g \mu_s)} \quad (2.41)$$

However, presence of higher order term increases nonlinearity. Figure 2.22 shows the nature of L versus l_g curve. It is possible to have two coils in the variable inductance transducer such that inductance in one coil increases and that in the other decreases. This can be adapted in the plunger type design, discussed later, where a push-pull arrangement of the coils and their connections would produce an output which is the sum of the fractional changes in the values of inductances in the two coils. This would make the even order terms in Eq. (2.40b) disappear and result in improvement of linearity over a wider gap range as shown in Figs. 2.23(a) and (b).

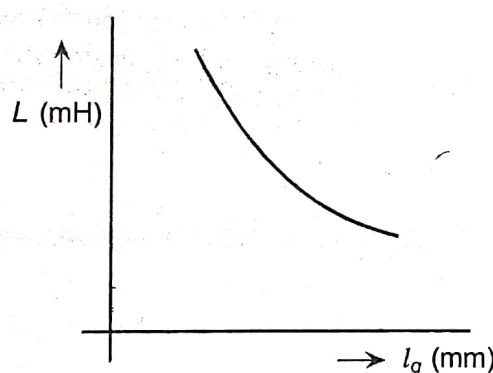


Fig. 2.22 Variation of inductance with air gap.

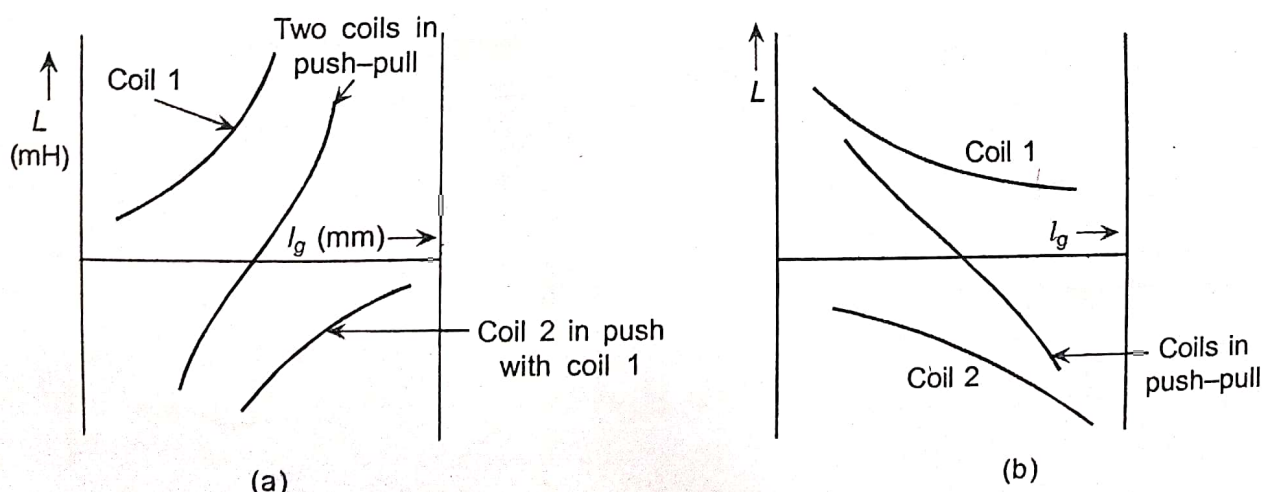


Fig. 2.23 Linearity improvement by using two coils in push-pull.

It must be remembered that air gap is likely to vary because of the eddy loss effect that is assumed parallel to the inductance which when transferred to series path, is given by

$$R_{es} = R_e(1 + Q^2)^{-1} \approx \frac{R_e}{Q^2} \quad (2.42)$$

As Q contains L as well as frequency f and L being a functions of μ , the resistance R_{es} changes with change in μ or in air gap. The values can actually be computed by using the equations that have been discussed here.

2.4.4 The Transformer Type Transducer

The transformer type transducer can be formed like a transformer with a variable iron core coupling between a pair of coils or more. Figures 2.17(d)(i) and (ii) show two such kinds, of which the latter one can be considered as a typical case where one coil acts as a primary (in which an ac voltage is impressed) and the other acts as the secondary. But for this type, there often occurs a 'no signal' output and this can be compensated by another coil or a compensating current. In this group, the transducer used most is the linear variable differential transformer (LVDT) whose operation has been described in detail later in the book. In LVDT, a plunger type armature moves into a pair of secondary coils and a primary coil, the secondaries being connected in differential mode. The simple plunger type sensor has also been thoroughly discussed in Chapter 4.

While LVDT in the Chapter 4 on Magnetic sensors has been analyzed using an equivalent circuit of a transformer, basic equations are quoted here without the complex deduction process. It takes help of the properties of the magnetic circuit and flux leakages. It has been assumed that the mmf in ferromagnetic/iron is negligible in comparison with that in air paths of the leakage flux. Figure 2.30 is a schematic representation of the differential transformer. For magnetic circuit-based deduction, the gaps and material dimensions are very important.

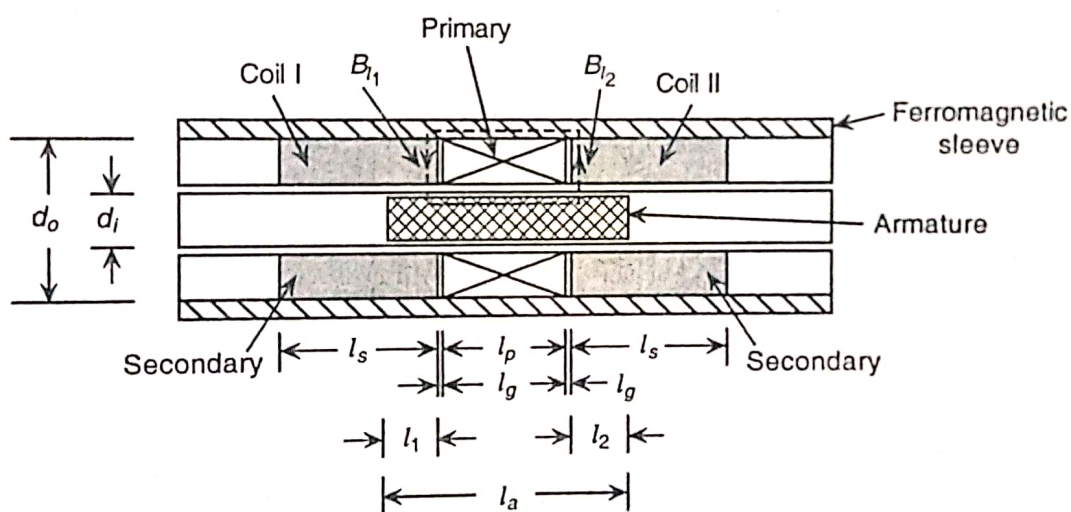


Fig. 2.30 The linear variable differential transformer.

Assuming current in the primary as I_p (rms) and number of turns n_p , if the number of turns in each secondary is n_s , it can be shown that the flux densities around the primary coil linking the secondaries are given as

$$\frac{B_L}{B_l} = -\frac{2l_2 + l_g}{2l_1 + l_g} \quad (2.60)$$

The negative sign comes because of direction (see Fig. 2.30).

For a supply frequency ω , the induced emf's in coils I and II are given respectively by

$$e_1 = \frac{2\pi^2 \omega I_p n_p n_s}{\ln(d_o/d_i)} \cdot \frac{2l_2 + l_g}{l_s l_a} \cdot x_1^2 \times 10^{-7} \quad (2.61a)$$

and

$$e_2 = \frac{2\pi^2 \omega I_p n_p n_s}{\ln(d_o/d_i)} \cdot \frac{2l_1 + l_g}{l_s l_a} \cdot x_2^2 \times 10^{-7} \quad (2.61b)$$

where x_1 and x_2 represent penetration of armature from nominal position beyond the primary coil length including the air gap.

Thus, the differential voltage

$$e_o = e_1 - e_2 = \left[\frac{2\pi^2 \omega I_p n_p n_s}{\ln(d_o/d_i)} \times 10^{-7} \right] \frac{l_g}{l_s l_a} \left[\left(\frac{2l_2}{l_g} + 1 \right) x_1^2 - \left(\frac{2l_1}{l_g} + 1 \right) x_2^2 \right] \quad (2.62a)$$

$$= K_1 \left[\left(\frac{2l_2}{l_g} + 1 \right) x_1^2 - \left(\frac{2l_1}{l_g} + 1 \right) x_2^2 \right] \quad (2.62b)$$

$$= K_1 \left[x_1^2 - x_2^2 + \left(\frac{2}{l_g} \right) (l_2 x_1^2 - l_1 x_2^2) \right] \quad (2.62c)$$

where

$$K_1 = \left(\frac{2\pi^2 \omega I_p n_p n_s}{\ln(d_o/d_i)} \right) \frac{l_g}{l_s l_a} \times 10^{-7}$$

In normal condition, if $l_1 = l_2 = l$, then

$$e_o = K_1 \left(1 + \frac{2l}{l_g} \right) (x_1^2 - x_2^2) \quad (2.63)$$

Approximate linearization is done by making $(1/2)(x_1 + x_2) = x_0 = \text{constant}$, and $(1/2)(x_1 - x_2) = x$, the weighted differential movement, then

$$\begin{aligned} e_o &= \left[4K_1 \left(1 + \frac{2l}{l_g} \right) x_o \right] x \\ &= K_2 x \end{aligned} \quad (2.64)$$

A rearrangement of Eq. (2.61) converts e_o in the form

where

$$e_o = K_3 x (1 - K_4 x^2) \quad (2.65)$$

$$K_3 = \frac{8\omega I_p n_p n_s (l_p + 2l_g + x_o) x_o \times 10^{-7}}{\ln(d_o/d_i) \cdot l_s l_a} \quad (2.66a)$$

$$K_4 = \frac{1}{(l_p + 2l_g + x_o) x_o} \quad (2.66b)$$

In fact, there is a nonlinearity in the output which is given by the relation

$$\eta_l = K_4 x^2 \quad (2.67)$$

Assuming that $2l_g \ll l_p$ and that even at maximum movement the armature remains within the secondary coils, one can simplify the output relation as

$$e_o = \left(\frac{8\pi^2 \omega I_p n_p n_s}{\ln(d_o/d_i)} \right) \frac{2l_p}{3l_s} \left(1 - \frac{x^2}{2l_p^2} \right) \times 10^{-7} \quad (2.68)$$

The maximum movement of x , x_{\max} , l_p , and l_s can now be given for a given nonlinearity.

With iron core, power frequency is usually preferred although a frequency of upto about 5000 Hz can be used with sufficient accuracy. Above this, the core loss rises enormously. This core loss even at lower frequencies creates a different problem—a non-zero output at balance condition mainly because of dissimilar losses due to harmonic contents and varying capacitive effects.

2.4.5 Electromagnetic Transducer

It is a bilateral double-function type transducer, as has already been mentioned, that has ‘mechanical input–electrical output’ and ‘electrical input–mechanical output’ construction.

A general name of such systems is *electromechanical energy converters* which are governed simultaneously by (i) Faraday’s law of electrodynamics and (ii) piezoelectric effect as postulated by Curie. Such transducers can be used both as ‘generators’ and ‘sensors’ often termed as ‘senders’ and ‘receivers’ respectively. Only the latter usage is of relevance here and is discussed.

Similar to the reluctance type transducer, such a system consists of an inductance coil wound on a ferromagnetic core and a variable gap provides the variation in the output. For producing unidirectional flux, a magnetizing coil with a bias current may be provided or the core can itself be a permanent magnet. Generally, a permanent magnet is used as a core.

If a coil of n turns wound on the core has a coil flux ϕ and coil inductance L , then as shown earlier

$$L = \frac{\mu_0 a n^2}{d} \quad (\text{H}) \quad (2.69)$$

for coil cross-section a , the effective gap d is given by (refer Fig. 2.31)

$$d = x_1 + \left(\frac{\mu_1}{\mu_2} \right) l_1 \quad (2.70)$$

μ_1 and μ_2 being relative permeabilities of air and core material respectively. Usually μ_1 is unity. Also the magnetic energy stored in the coil is

$$E_m = \frac{1}{2} \frac{(n\phi)^2}{L} \quad (2.71)$$

If a current

$$I = \frac{n\phi}{L} \quad (2.72)$$

flows in the coil, the stored energy is obtained by combining Eqs. (2.69), (2.71) and (2.72) as

$$E_m = \frac{1}{2} \frac{\mu_0 I^2 a n^2}{d} \quad (2.73a)$$

$$= \frac{1}{2} L I^2 \quad (2.73b)$$

This energy leads to development of a force f across the gap d (sign ignored) as

$$f = \frac{\partial E_m}{\partial d} = \frac{1}{2} \frac{L I^2}{d} \quad (\text{N}) \quad (2.74)$$

which would consist of a number of components depending on the 'magnetic condition' of the core. If the bias magnetizing current or its equivalent is given by I_o and a sinusoidal current of amplitude of i and frequency ω with $i \ll I_o$ energizes the core, then (ignoring the i^2 terms)

$$f = \left(\frac{L}{2d} \right) (I_o^2 + 2I_o i) \quad (2.75)$$

If the coil resistance is negligible, then

$$i = \frac{V}{j\omega L} \quad (2.76)$$

and the varying force term is

$$f_v = \frac{L I_o}{d} \cdot i \quad (2.77a)$$

and using Eq. (2.76)

$$f_v = \frac{I_o V}{j\omega d} \quad (2.77b)$$

The force f is associated with a velocity v as shown in Fig. 2.31 so that with analogy of electrical parameters, we can write

$$f_m = Z_m v \quad (2.78)$$

where Z_m is the mechanical impedance.

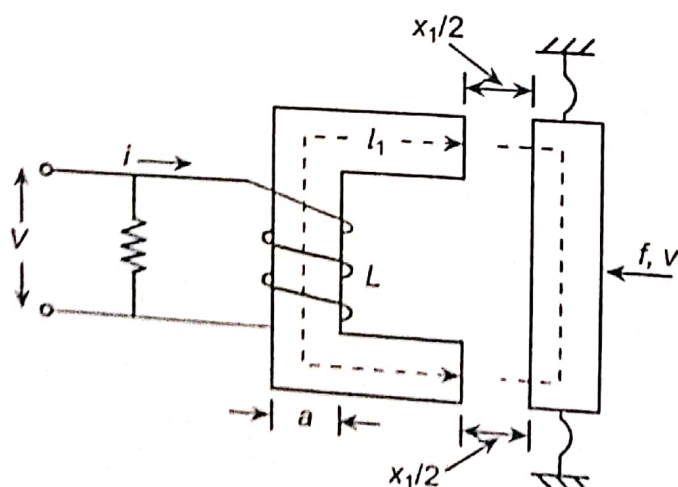


Fig. 2.31 Double-function electromagnetic transducer.

If m , k , and δ represent the mass, stiffness, and damping of the transducer (mechanical), then

$$Z_m = \delta + j\left(\omega_m - \frac{k}{\omega}\right) \quad (2.79)$$

Equations (2.77b) and (2.78) may be combined to give

$$f_t = Z_m v \frac{I_o V}{j\omega d} \quad (2.80)$$

A relation between voltage V , velocity v , and current i can be written as

$$V = \alpha_{vv} v + \alpha_{iv} i \quad (2.81)$$

where α_{iv} is the electrical impedance and α_{vv} is complex transducer coefficient. Equation (2.81) can also be used to write, v in terms of V and i .

It can be shown that 'receiver' has a voltage to force ratio

$$\frac{V}{f} = \frac{I_o / (j\omega d)}{\left(\frac{I_o^2}{\omega^2 d^2} \right) + \left(\delta + j\left(\omega_m - \frac{k}{\omega}\right) \right) \left(\frac{1}{R} + \frac{1}{R_o} + \frac{1}{j\omega L} \right)} \quad (2.82)$$

Where R_o is the load (indicator) resistance and is large, and R is the coil resistance (considered parallel to inductance). The characteristic transfer matrix equation of the transducer can be written as

$$\begin{bmatrix} f \\ v \end{bmatrix} = \begin{bmatrix} \frac{I_o}{j\omega d} & 0 \\ -d & \frac{j\omega d}{L I_o} \end{bmatrix} \begin{bmatrix} V \\ i \end{bmatrix} \quad (2.83)$$

To this, the mechanical impedance and electrical impedances are superposed so that we get V/f as given by Eq. (2.82).

2.4.6 Magnetostrictive Transducer

Magnetostrictive transducer is not popular as a transducer mainly because of its limitations with respect to materials. Besides the input quantity, its output depends on some other variables also. It is of two different types, namely (i) the variable permeability type and (ii) the variable remanence type.

In general, a magnetostrictive material such as pure nickel has a slope of the hysteresis curve that decreases with increasing tension σ , as shown in Fig. 2.32. This change alters the value of the permeability μ , which also decreases with stress and hence, inductance of a coil wound on it. Also, with increasing tension, the remanence magnetism B_0 decreases. Ni is seen to be a material with negative magnetostriction.

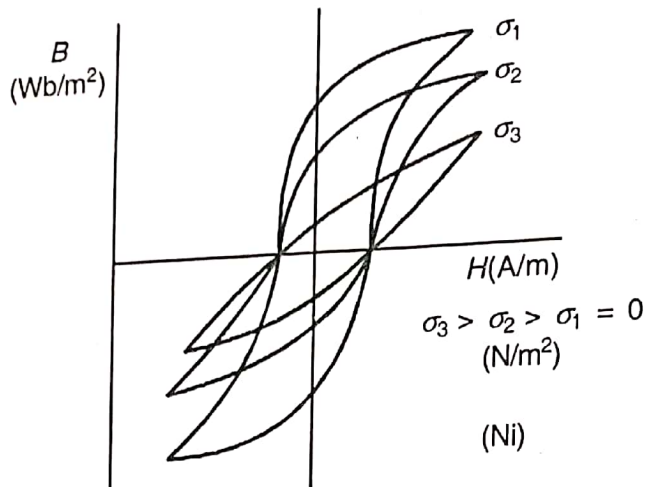


Fig. 2.32 B - H loops of magnetostrictive material with changing tension.

However, in case of Ni-Fe alloy known as permalloy such as 68 permalloy (Ni 68), 45 permalloy (Ni 45), the picture is reversed. Increasing tension increases B_0 as also permeability. The shapes of the B - H curves for such a situation are depicted in Fig. 2.33.

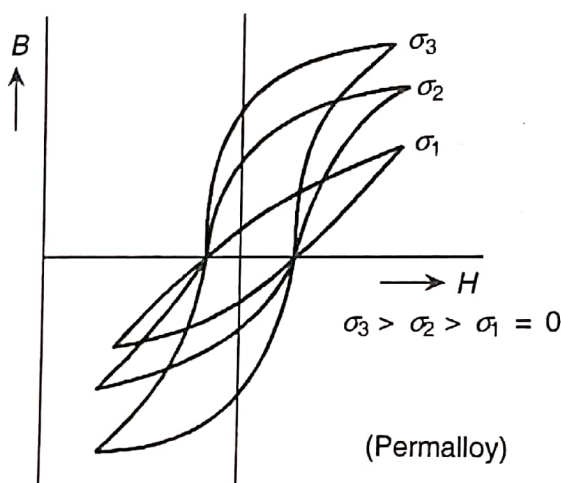


Fig. 2.33 B - H loops of another type of material with varying tension.

A typical scheme of the transducer using variable permeability is shown in Fig. 2.34(a). The coil inductance changes with change of force as the latter changes the core permeability. The coil inductance is measured through a bridge with the current and frequency, the coil also changes the inductance. These quantities and temperature have to be kept under strict regulation.

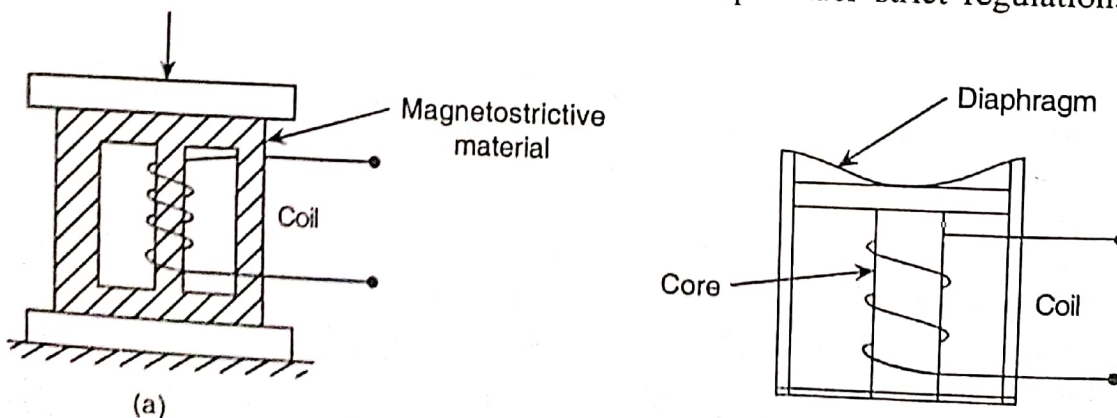


Fig. 2.34 (a) Scheme of a sensor with magnetostrictive material, (b) transducer operated by a diaphragm usually used in accelerometers.

The variable remanence type transducer is used for specific applications such as an accelerometer where the transducer is designed to receive the stress through a metal diaphragm as shown in Fig. 2.34(b). The open circuit voltage is proportional to the rate of change of the remanence magnetism. In fact, a relation is given as

$$B_0 - B_{0i} = k_1 \sigma \quad (2.84)$$

and for n turns of coil, the output voltage V is

$$V = nk_2 \frac{dB_0}{dt} \quad (2.85)$$

The k_i 's in these equations are constants.

2.4.7 Materials—Some Comments

The core and armature material is essentially ferromagnetic that has high permeability, low loss, high Curie temperature, and low cost. Soft magnetic Ni–Fe alloy is good for the purpose in which there are a few commercial variety such as (i) Mu-metal and (ii) Radiometal (radiometal can further be subdivided into a few types). The permeability in the two cases varies as 60×10^3 to 240×10^3 and 4×10^3 to 65×10^3 respectively. Hysteresis losses are 4 and $40 \text{ J/m}^3/\text{cycle}$ respectively while Curie temperatures are 350° and 540°C respectively.

Magnetically soft ferrites consisting of mixed crystals of cubic ferrites are good alternatives, which again have a number of varieties represented by the general formula $M\text{Fe}_2\text{O}_4$ where M is a divalent metal such as manganese–zinc, magnesium–zinc, nickel–zinc, and so on. Such materials have initial permeabilities varying from 0.7×10^3 to 1.8×10^3 . One special feature is that ferrites have resistivities about 10^6 times higher than ferromagnetics such that the eddy losses are negligible. Some of such ferrites can be used in high frequency ranges, for example, the Ni–Zn ferrite is particularly suitable for the purpose.

2.5 CAPACITIVE SENSORS

Three types of capacitive sensors can be listed under this category, namely

1. variable capacitance type with varying distance between two or more parallel electrodes (Fig. 2.35(a)).
2. variable capacitance obtained by variable area between the electrodes. An interesting variation of this is obtained by making serrated electrodes or electrodes with teeth, one of which moves (Fig. 2.35(b)), and
3. variable capacitance obtained by having variable dielectric constant of the intervening material. For this the material has to move between the pair of electrodes, and the change in capacitance is obtained and measured (Fig. 2.35(c)).

A fourth variety, the piezoelectric type, depends on the piezoelectric properties of specific kinds of dielectric materials and would be considered later. The movement of the moving electrode of the type shown in Fig. 2.35(b) is restricted to be short, while that of the dielectric material such as an insulation tape is not restricted.

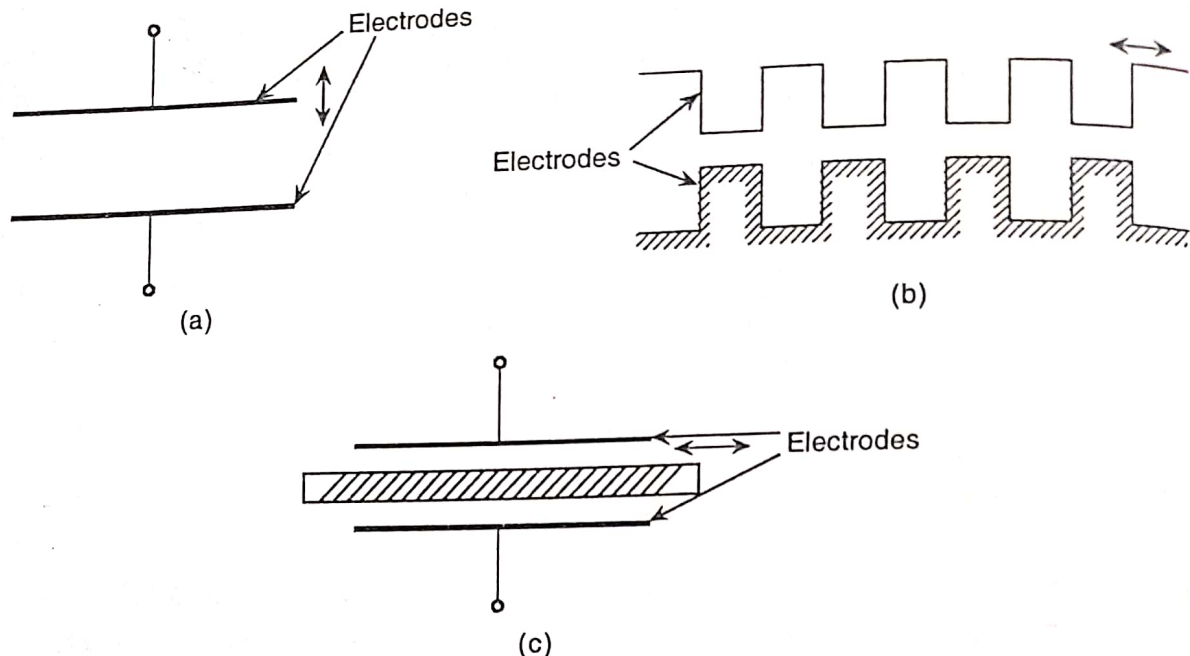


Fig. 2.35 (a) Parallel plate capacitance type, (b) capacitance type with serrated electrodes, and (c) capacitance type with varying dielectric type material.

A variation in parallel type design is the cylindrical design. Besides, the parallel plate capacitive sensor is often used in a differential form with three plates as shown in a Fig. 2.36(a). For a parallel plate capacitor with dielectric constant or permittivity ϵ , which is the product of its relative permittivity and the permittivity of the free space (vacuum, often taken as air) of value 8.85×10^{-12} F/m and plate area α , each separated by a distance x from the other, the capacitance is

$$C_p = \frac{\epsilon \alpha}{x} \quad (2.86)$$

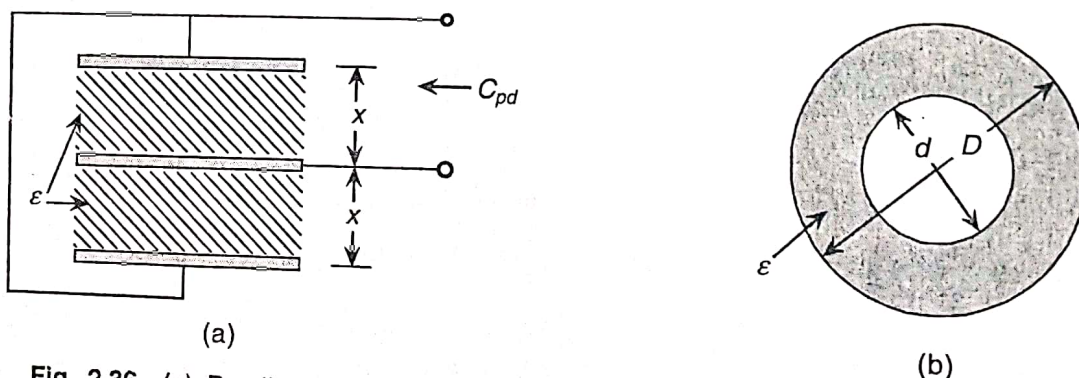


Fig. 2.36 (a) Parallel plate capacitance sensor, using three plates, (b) cylindrical type capacitance sensor.

A typical three plate capacitor arrangement is shown in Fig. 2.36(a). The capacitance C_{pd} is then given as

$$C_{pd} = \frac{2\epsilon \alpha}{x} \quad (2.87)$$

For the cylindrical sensor with the electrode thickness negligible as compared to dielectric thickness (Fig. 2.36(b)), the capacitance is

$$C_c = \frac{2\pi\epsilon l}{\ln(D/d)} \quad (2.88)$$

where l is the cylinder length.

For very thin layer of dielectric material, Eq. (2.88) can be approximated to

$$C_{ca} = \frac{\pi\epsilon l(D+d)}{(D-d)} \quad (2.89)$$

If in a parallel plate pair the dielectric has a number of layers of dielectric constants with corresponding permittivity ϵ_i for thickness x_i , the relation (2.86) can be modified to

$$C_{pi} = \frac{\alpha}{\sum x_i/\epsilon_i} \quad (2.90)$$

The capacitance is, in general, associated with a high resistance, called *leakage*, because the dielectric materials do not have infinite permittivity. This leakage is represented by a parallel resistance R_p , particularly at lower frequencies of measurement. This loss consists of dc conductance, dielectric loss of insulators supporting the electrodes, and the actual dielectric loss. With increasing frequency, the load resistances R_l contribute to loss factors and the complete equivalent circuit is given by the circuit of Fig. 2.37, where the inductance L represents the inductance between the terminals as also the cable inductance whenever such cable is used. Such an equivalent circuit would be taken up at a later stage.

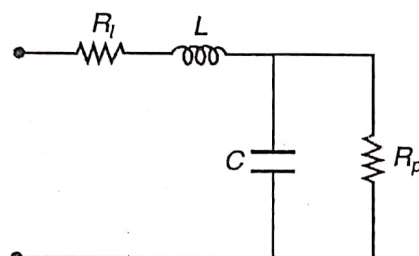


Fig. 2.37 Equivalent circuit of the capacitance transducer.

2.5.1 The Parallel Plate Capacitive Sensor

Considering now a general case of a pair of parallel plates with a solid dielectric of a certain thickness x_s and an air gap x_a as shown in Fig. 2.38, the capacitance C is given by

$$C = \frac{\alpha}{\left(\frac{x_a}{\epsilon_a}\right) + \left(\frac{x_s}{\epsilon_s}\right)} \quad (2.91)$$

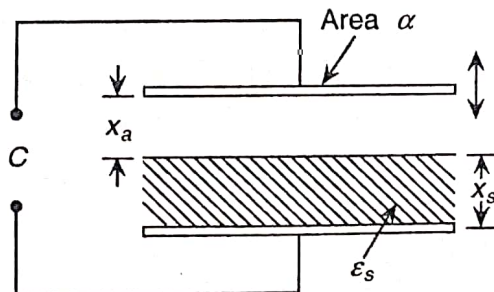


Fig. 2.38 Parallel plate sensor with different dielectric materials.

With the plate moving, a decrease in x_a increases C and vice versa. Thus,

$$C \pm \partial C = \frac{\alpha}{\left(\frac{x_a \mp \partial x_a}{\epsilon_a} + \frac{x_s}{\epsilon_s} \right)} \quad (2.92)$$

Considering, however, $\epsilon_a \approx 1$, for simplicity, we obtain

$$\mp \frac{\partial C}{C} = \pm \left(\frac{\partial x_a}{x_a + x_s} \right) \left(\frac{1}{1 + \frac{x_s}{x_a \epsilon_s}} \mp \frac{\partial x_a}{x_a + x_s} \right) \quad (2.93)$$

In Eq. (2.93), the quantity $(1 + x_s/(x_a \epsilon_s))/(1 + x_s/x_a)$ is an important factor in determining the value of $\pm \partial C/C$ as well as its nature. This quantity is represented as $1/\beta$, where β is often referred to as the *sensitivity factor*, but it also is responsible for the nonlinearity. Writing $(\partial x_a/x_a)/(1 + x_s/x_a) = (\partial x_a/x_a)/(1 + \lambda)$, $\pm \partial C/C$ can be expanded as

$$\mp \frac{\partial C}{C} = \pm \left(\frac{\partial x_a}{x_a} \right) \left(\frac{\beta}{1 + \lambda} \right) \left[1 \pm \left(\frac{\partial x_a}{x_a} \frac{\beta}{1 + \lambda} \right) + \left(\frac{\partial x_a}{x_a} \frac{\beta}{1 + \lambda} \right)^2 \pm \dots \right] \quad (2.94)$$

As β is a function of x_a , x_s , and ϵ_s , the plots of β versus λ with ϵ_s as a parameter show that with increasing λ , β increases with ϵ_s , its minimum value being 1 for $\epsilon_s = 1$.

It must be stressed here that capacitors have fringing effects which are usually taken care of by providing guard ring which is a ring surrounding a plate of the capacitor, the ring and the plate both being at the same potential.

2.5.2 Serrated Plate Capacitive Sensor

As has been discussed earlier, a pair of flat serrated plates, one of which is fixed in position, the other with a small relative movement show change in capacitance and this principle is utilized in some cases to measure small angular variations. For the measurement to be of any significance, the relative movement has to be small. Figure 2.39 shows the active tooth length (on the fixed plate) as l , air gap as x , tooth width as w ; if number of teeth-pair is n and air permittivity is ϵ_a , the capacitance C is given as

$$C = \frac{\epsilon_a l w n}{x} \quad (2.95)$$

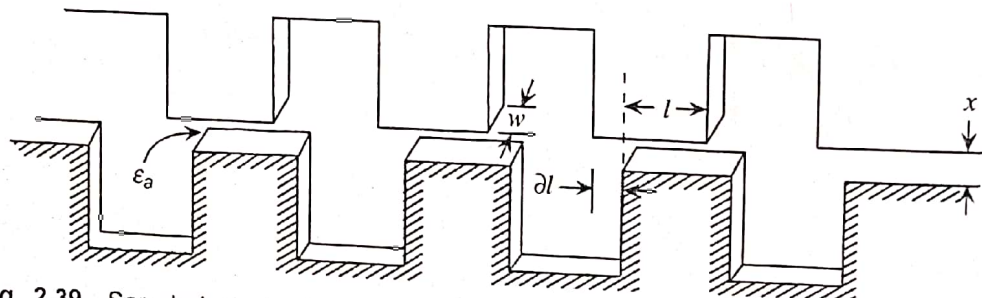


Fig. 2.39 Serrated electrode capacitance sensor with changing active tooth length.

so that for a small relative movement ∂l of the moving plate, we obtain

$$\frac{\partial C}{C} = \frac{\partial l}{l} \quad (2.96)$$

This simplified relation assumes no fringing effect. However, by drawing actual equipotential lines and parallel flux lines between the pair of teeth, the leakage can be allowed in the relation. Therefore, Therefore,

$$\frac{\partial C}{C} = \frac{\partial l}{l} \left(\frac{1}{1 + \frac{kx}{l}} \right) \quad (2.97)$$

where the expression within the brackets can be termed as the sensitivity factor, β_s , which decreases with increasing x/l as shown in Fig. 2.40. This factor β_s is actually the ratio of nonleakage to total flux.

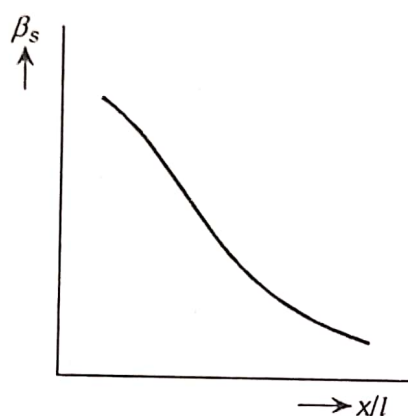


Fig. 2.40 Sensitivity versus normalized gap curve.

2.5.3 Variable Permittivity or Variable Thickness Dielectric Capacitive Sensor

This type of capacitive sensors can be represented as shown in Fig. 2.41. With plate effective area α and other dimensions as shown in the figure, the capacitance C is given by

$$C = \frac{\alpha}{l - x + \frac{x}{\epsilon_d}} \quad (2.98)$$

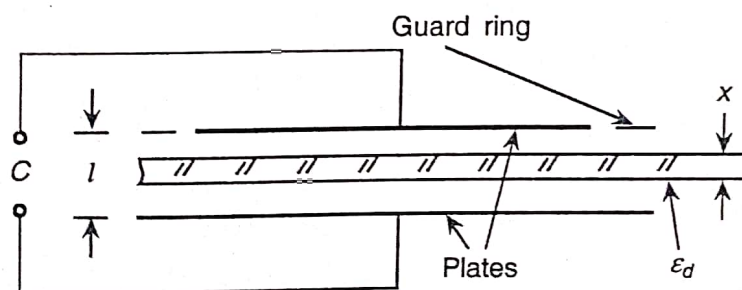


Fig. 2.41 Scheme of a variable permittivity (or thickness) dielectric type sensor.

where ϵ_d is the permittivity of the dielectric material. Following the development in Section 2.5.1, one obtains the normalized change in capacitance as

$$\left(\frac{\partial C}{C}\right)_{\epsilon_d} = \pm \frac{\partial \epsilon_d}{\epsilon_d} \frac{1/[1 + \epsilon_d(l-x)/x]}{1 \pm \frac{1}{1 + x/(\epsilon_d(l-x))}} \cdot \frac{\partial \epsilon_d}{\epsilon_d} \quad (2.99)$$

Here, $1/(1 + \epsilon_d(l - x)/x)$ is the sensitivity factor β_s and the nonlinearity factor is $\eta_n = 1/(1 + x/(\epsilon_d(l - x)))$. If $\eta_n \partial \epsilon_d / \epsilon_d$ is small, we obtain, with first order approximation,

$$\left(\frac{\partial C}{C}\right)_{\epsilon_d} = \frac{\partial \epsilon_d}{\epsilon_d} \cdot \frac{1}{1 + \epsilon_d(l - x)/x} \left[1 \mp \frac{\partial \epsilon_d / \epsilon_d}{1 + x/(\epsilon_d(l - x))} \right] \quad (2.100)$$

Obviously, with $x/(l - x)$ high, β_s is high and η_n is low which must be a good choice.

Instead of variation in ϵ_d , there may be variation in x , so that we have

$$\left(\frac{\partial C}{C}\right)_x = \frac{\partial x}{x} \frac{\frac{\epsilon_d - 1}{1 + \epsilon_d(l - x)/x}}{1 \mp \frac{\epsilon_d - 1}{1 + \epsilon_d(l - x)/x} \frac{\partial x}{x}} \quad (2.101)$$

and if $[(\epsilon_d - 1)/(1 + \epsilon_d(l - x)/x)] \partial x / x \ll 1$, taking the first order term only, the expression for $(\partial C/C)_x$ is obtained as

$$\left(\frac{\partial C}{C}\right)_x = \frac{\partial x}{x} \frac{\epsilon_d - 1}{1 + \epsilon_d(l - x)/x} \left[1 + \frac{\epsilon_d - 1}{1 + \epsilon_d(l - x)/x} \frac{\partial x}{x} \right] \quad (2.102)$$

In this case, the sensitivity factor and the nonlinearity factor are identical and given by $(\epsilon_d - 1)/(1 + \epsilon_d(l - x)/x)$. It means that the sensitivity is good with high $x/(l - x)$ as also ϵ_d , but the nonlinearity also increases.

A diaphragm formed by machining from the solid to avoid large hysteresis losses is said to be clamped type and although it may be made to have its thickness small enough with respect to its diameter, it does provide a stiffness to bending. If the diaphragm thickness is τ and material Poisson's ratio ν , Young's modulus Y , for other dimensions as shown in Fig. 2.42, the deflection x is given by

$$x = \frac{3p}{16} \cdot \frac{1 - \nu^2}{Y\tau^3} (R^2 - r^2)^2 \quad (2.109)$$

Following the similar procedure as above, the sensitivity may be derived as

$$\frac{\partial C}{C} = \frac{(1 - \nu^2) R^4}{16 Y l t^3} p \quad (2.110)$$

2.5.5 Electrostatic Transducer

Similar to the electromagnetic transducer discussed in Section 2.4.5, capacitive type transducer can also be developed with bilateral characteristics, where it is used with dc polarization. Such a transducer is also referred to as an *electrostatic transducer*. A typical scheme of such a system is shown in Fig. 2.43. A capacitor is formed with a 'flexible' diaphragm which can move due to application of force and a rigid plate p_1 . There is bias voltage V_s which is sufficiently large. When the system acts as a transducer, the gap x between the plates changes as by some pressure in case of an 'electrostatic microphone'. This pressure may be considered sinusoidal in nature for analysis purpose. A circuit consisting of a resistance R and capacitance C 'varying sinusoidally' allows V_s to send a sinusoidal current i to flow in it and hence, a sinusoidal output V_o across resistance R is obtained.

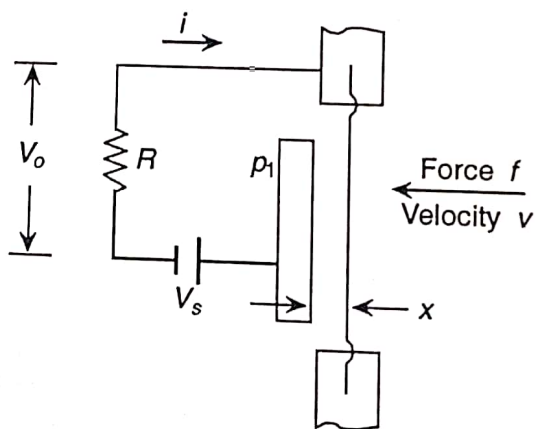


Fig. 2.43 Electrostatic transducer.

Analyzing as in the case of electromagnetic transducer, V_o corresponding to a force f can be obtained in terms of the parameters V_s , x , R , C , ω , mass m , stiffness k , and damping (ζ) of the system. In fact, the dynamic transfer function is given by

$$\frac{V_o(s)}{f(s)} = \frac{s x_o / R C_o V_s}{s^3 x_o^2 m R C_o + s^2 (m x_o^2 + x_o^2 R C_o \zeta) + s (x_o^2 \zeta + x_o^2 R C_o k) + (x_o^2 k + V_s^2 C_o)} \quad (2.111)$$

where, C_o and x_o are the initial values of x and C , and s may be replaced by $j\omega$ where ω is the input circular frequency.

Frequency response analysis of this shows a flat response upto a frequency $\omega_o = (k/m)^{1/2}$, at which a resonance occurs and range is obviously specified by the same. Also below $\omega_b = (C_o R)^{-1}$, the response is not constant. Hence, the frequency range is $(\omega_o - \omega_b)$.

In case of generating action, alongwith bias V_s , a sinusoidal input voltage is also applied so that the diaphragm undergoes electrostatic vibration.

2.5.6 Piezoelectric Elements

Crystals of certain classes are said to show piezoelectric effect which essentially means electric polarization produced by mechanical strain in the crystals. Such a polarization is believed to occur because of asymmetric crystal structure. The effect is reversible in the sense that a strain may be produced in the crystal by electrically polarizing it using an external source. While the mechanical input to electrical output form is used in developing transducers extensively, the reverse effect is used in many modern gadgets such as sonar systems, ultrasonic non-destructive test equipment, ultrasonic flowmeters, pump for inkjet printers, and so on.

Also a piezoelectric crystal is represented by a set of three Cartesian coordinates so that the polarization P can be represented in the vector form as

$$\mathbf{P} = P_{xx} + P_{yy} + P_{zz} \quad (2.112)$$

However, P_{xx} , P_{yy} , and P_{zz} are again related to the stresses, axial and shear, σ , and χ , in terms of a set of axes-dependent coefficients called d -constants of the crystal. With the axial and shear axes as shown in Fig. 2.44 with reference to the crystal axes X-Y-Z, we obtain

$$\begin{bmatrix} P_{xx} \\ P_{yy} \\ P_{zz} \end{bmatrix} = \begin{bmatrix} d_{11} & d_{12} & d_{13} & d_{14} & d_{15} & d_{16} \\ d_{21} & d_{22} & d_{23} & d_{24} & d_{25} & d_{26} \\ d_{31} & d_{32} & d_{33} & d_{34} & d_{35} & d_{36} \end{bmatrix} \begin{bmatrix} \sigma_{xx} \\ \sigma_{yy} \\ \sigma_{zz} \\ \chi_{yz} \\ \chi_{zx} \\ \chi_{xy} \end{bmatrix} \quad (2.113)$$

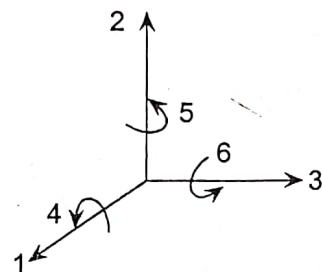
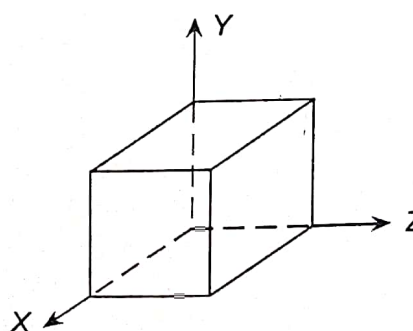


Fig. 2.44 The piezoelectric crystal defined in X-Y-Z axes.

The d -constants are defined as

$$d_{ij} = \frac{\text{charge generated in direction } i}{\text{force applied in direction } j} = \frac{Q_i}{f_j} \quad (2.114)$$

expressed as coulomb per Newton usually. The reverse effect *d*-coefficients are similarly defined as

$$d_{ij} = \frac{\text{strain in direction } i}{\text{field applied in direction } j} = \frac{\varepsilon_i}{E_j} \quad (2.115)$$

expressed usually in (m/m)/(V/m).

One other coefficient which is of importance in practical design is the *g*-coefficient and is related to the *d*-coefficient by the dielectric constant of the material. It is defined as the voltage gradient or field in the crystal per unit pressure imparted to it. Maintaining the direction as before, it can be shown that

$$g_{ij} = \frac{Q_i}{\varepsilon_d f_j} = \frac{d_{ij}}{\varepsilon_d} \quad (2.116)$$

A third coefficient, the *h*-coefficient, is defined as the voltage gradient per unit strain which also appears to be the reciprocal of *d*_{ij} given by Eq. (2.115). The *h*-coefficient is easily obtained from the *g*-coefficient by multiplying it with the Young's modulus in the appropriate direction.

Crystals, for various uses, are characterized by coupling coefficient which actually is a measure of the efficiency of the crystal as energy converter. Its application in transducer engineering is limited but it is a necessary parameter when used in generators.

The numerical value of coupling coefficient is given by

$$K_{ij} = (d_{ij} h_{ij})^{1/2} \quad (2.117)$$

The value of *d*₁₁ for quartz is 2.3×10^{-12} coulombs/N and its dielectric constant is 4.06×10^{11} F/m. Hence, its *g*₁₁ value is 56×10^{-3} (V/m)/(N/m²).

Piezoelectric materials

Materials for piezoelectric sensors have been divided into two groups: (i) those occurring naturally such as quartz, rochelle salt $\text{NaKC}_4\text{H}_4\text{O}_6 \cdot 4\text{H}_2\text{O}$, tourmaline and so on, (ii) those produced synthetically such as lithium sulphate (LS), $\text{NH}_4\text{H}_2\text{PO}_4$ or ammonium dihydrogen phosphate (ADP), and BaTiO_3 or barium titanate (BT). Barium titanate is actually a ferroelectric ceramic and requires to be polarized before use. Besides, there are certain polymer films which also exhibit the piezoelectric property.

Crystals like quartz have natural asymmetric structure which is responsible for this property. Quartz is representable as a helix along which one silicon and two oxygen atoms interlace. The planar view of the crystal cell, perpendicular to the *z*-axis also called the optic axis, shows a hexagonal shape with one Si and two oxygen occupying the vertices alternately as shown in Fig. 2.45(a). The chemical structure gives the formula SiO_2 . In the normal unstressed condition, showing any electrical output.

However, with application of a force (compression) in the direction of *x*-axis, the crystal is deformed to the extent of being polarized so that positive and negative charges are generated as shown in Fig. 2.45(b). If this force is applied in the *Y*-direction, the deformation produced is such that opposite charges are now generated on the two faces as shown in Fig. 2.45(c). These two cases are known as longitudinal and transverse effects respectively. Changing the type of force, that is, from compression to tension, reversal in the polarity of charge generation occurs.

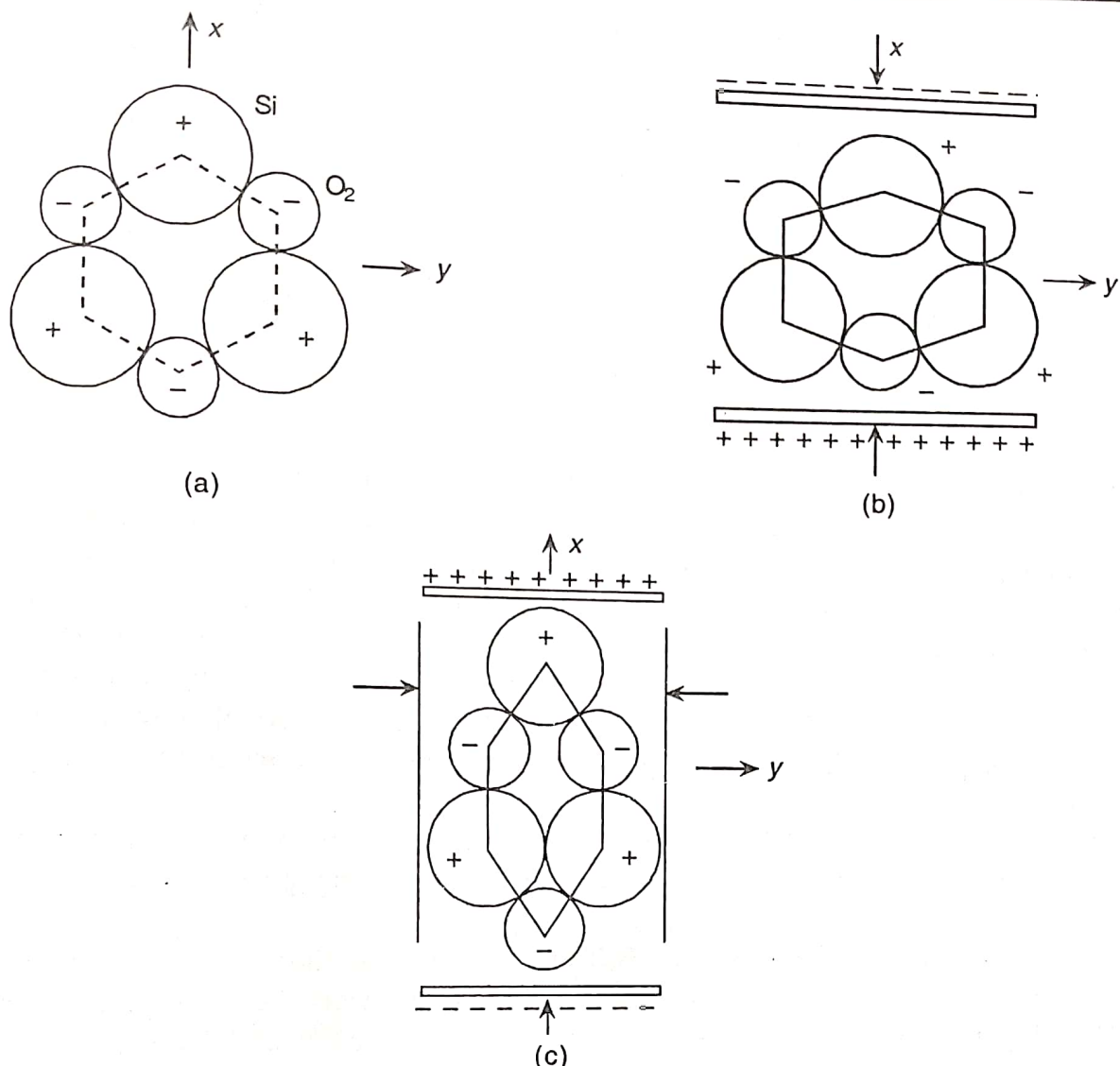


Fig. 2.45 (a) The quartz crystal model, (b) charge generation with force applied in the direction of the electrodes, and (c) charge generation with the force applied perpendicular to the position of electrodes.

As a result of the symmetry of the crystal structure in the z -direction, there does not occur any charge 'discrepancy' or polarization when force is applied in this direction and this axis is, therefore, termed as the *optic axis*.

It may be noticed that polarization deep inside the crystal is cancelled out and only the surface layers are affected to produce the free charges. The degree of distribution is thus, important for the amount of charges on the two faces which means that the force applied is the main criterion. This is true specially for the case of Fig. 2.45(b). However, in case of Fig. 2.45(c), the transverse charge 'size' in the x -direction has a multiplying factor α_x/α_y where α is the face area.

The material properties that are relevant to the piezoelectric sensors are (i) dielectric constant, (ii) d -coefficients (xx , say), (iii) resistivity (specifically, volume resistivity is considered), (iv) Young's modulus, (v) humidity range (since above or below this range large absorption of moisture occurs changing volume resistivity and performance characteristics), (vi) temperature range, and (vii) density. A comparative study of these properties is made in Table 2.5.

Table 2.5 Properties of piezoelectric materials

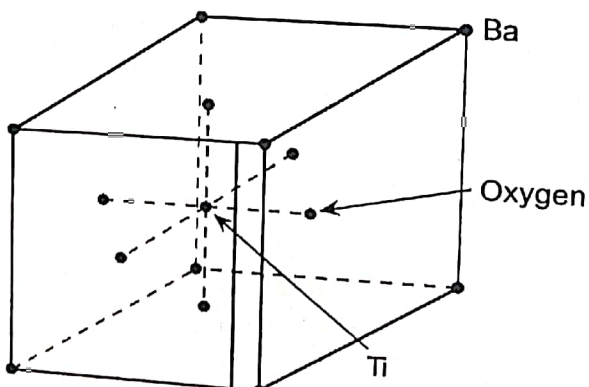
Material	d (relative)	$d_{xx} (\times 10^{-12})$ (cou/N)	ρ_v ($\Omega \cdot m$)	$Y (\times 10^9)$ (N/m ²)	H_R (%)	T_R (°C(max))	Density ($\times 10^3$) (kg/m ³)
Quartz	4.5	2.3	10^{12}	80	0-100	550	2.65
Rochelle Salt	350	550	10^{10}	10-20	40-70	45	1.77
Tourmaline	6.7	2-2.25	10^{11}	160	0-100	1000	3.10
LS	10.3	13-16	10^{10}	46	0-95	75	2.05
ADP	15.3	25-45	10^8	19.5	0-94	125	6.8
Titanates	500-1750	80-500	10^9-10^{13}	47-80	—	200-400	5.8-7.8

Inspite of some deficiencies such as low mechanical strength, limited humidity and temperature range, large hysteresis, and fatigue, Rochelle salt is often used in microphones and also in gramophone pickups because of high shear sensitivity and permittivity. Although available as naturally occurring, it is industrially grown now for bigger requirements.

Tourmaline has poor sensitivity ($d_{xx} \approx 2-2.5$) and is costly. It is, therefore, rarely used as a sensor of this type. But it has two specific advantages—(i) it has a long, perhaps the longest, volume-temperature range, and (ii) it is the only naturally occurring variety that shows large volume-expander mode capability, that is, with high force in all three directions it gives a large d -value in x - x direction.

Lithium Sulphate is good in volume-expander mode but ammonium dihydrogen phosphate is used quite extensively for acceleration and pressure sensing purposes although it has low permittivity. It can also be used in twisting applications.

Among the titanates, barium titanate ($BaTiO_3$)—a polycrystalline ceramic has high ϵ_d and with induced polarization is very conveniently used in many transducers. Ferroelectric materials can be analyzed analogous to the ferromagnetic ones and its polarization is effectively explained with the help of the ‘domain’ structure. The material is assumed to consist of ‘zones’ with spontaneous polarization (for example, Weiss zones in ferromagnetics) which can be partially oriented by the application of external electric field. A barium titanate crystal is modelled as shown in Fig. 2.46. The crystal cells are tetragonal with the axes ratio 1.01 and the central Ti atom has a preferred direction (120°C), the structure reduces to a cubic form and the polarizability is lost.

Fig. 2.46 The model of a $BaTiO_3$ crystal.

As in the case of soft magnetic material, ferroelectric material also loses polarization with time as the remanent polarization depends on the coercive force of the dipoles. This is understood from the hysteresis loop. This loss can be prevented and stability increased, by introducing polarization impurities such as lead, calcium, yttrium and so on. However, for transducers, lead zirconate titanate has been found to be more suitable than the simple ones suggested previously. Lead zirconate titanate is a solid solution of lead titanate and lead zirconate which is only 10–60 mole percent of the former. Depending on the amount of lead zirconate and also on processing techniques, values of d -coefficients differ greatly, the Curie point being pushed up in almost all the cases from 200° to 300° – 350°C . Another composition consists of lead actaniobate which has the highest Curie point.

The dielectric constant, d -coefficients, and dissipation in a ferroelectric ceramic change with temperature. The nature of such changes are shown in relative response plots in Fig. 2.47. These can be compared with those of quartz, specially the variation of d -coefficients and ε_d . Figure 2.48 shows the plots.

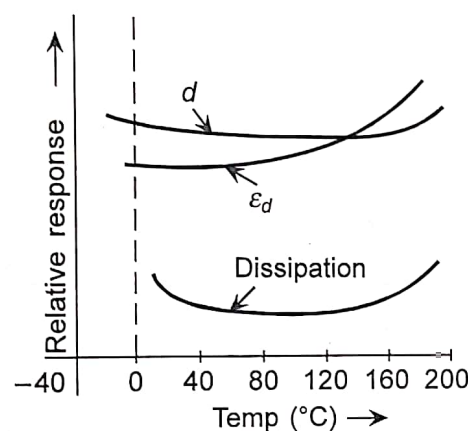


Fig. 2.47 Relative response-temperature curves for d -coefficients, dielectric constant and dissipation of BaTiO₃.

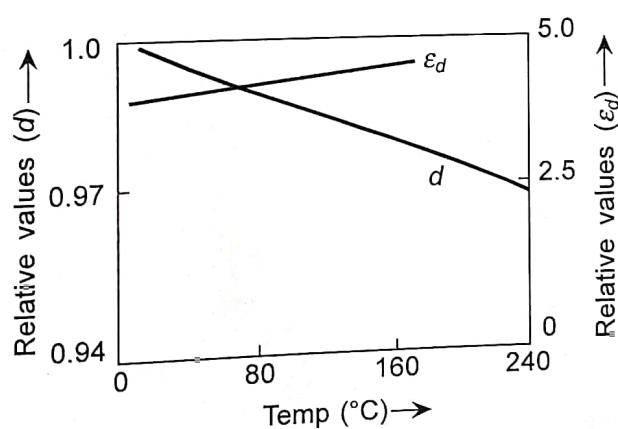


Fig. 2.48 Variation of d -coefficients, dielectric constant with temperature for quartz.

Titanates are synthetically produced by pressure, film-casting or extrusion, and finally sintering—the ohmic contacts are obtained by silver or palladium coating on which soldering of lead-wires can be done before polarization. Polarization is usually affected at a voltage of 2 KV/mm and is kept for a few minutes depending on the material.

Considering a quartz sensor of thickness t obtained by cutting perpendicular to its x -axis, two faces which have same areas (α each) and are perpendicular to this axis are metallized; if now, a force f_x is applied to it along the x -direction, the charge Q_x generated would be

$$Q_x = d_{11} f_x$$

The capacitance C_x of the sensor is then given by

$$C_x = \frac{\epsilon_d \alpha}{t} \quad (2.11c)$$

so that voltage V_x is

$$V_x = \frac{Q_x}{C_x} = \frac{d_{11} f_x t}{\epsilon_d \alpha} \quad (2.12c)$$

For a crystal of dimensions as shown in Fig. 2.49 with a force f_y in the y -direction, the charge on the plates perpendicular to x -direction is given by (as already mentioned)

$$Q_x = d_{12} \left(\frac{l_y}{l_x} \right) f_y \quad (2.12f)$$

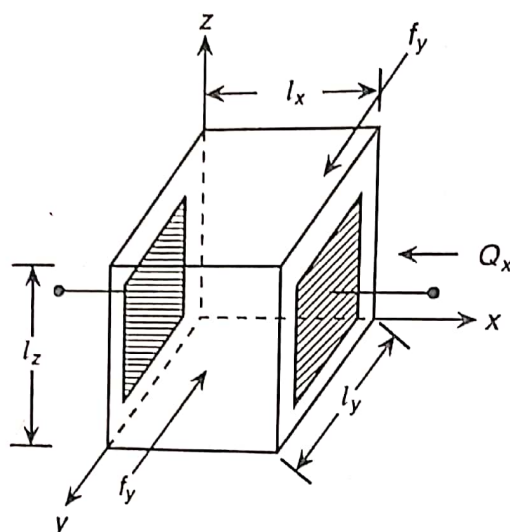


Fig. 2.49 A crystal with electrodes and marked dimensions.

However, for quartz, all the d -coefficients given in Eq. (2.113) are not finite nonzero values. In fact, the d -matrix for quartz is given as

$$[d] = \begin{bmatrix} d_{11} & -d_{11} & 0 & d_{14} & 0 & 0 \\ 0 & 0 & 0 & 0 & -d_{14} & -2d_{11} \\ 0 & 0 & 0 & 0 & 0 & 0 \end{bmatrix} \quad (2.122)$$

so that Eq. (2.121) is modified as

$$Q_x = -d_{11} \left(\frac{l_y}{l_x} \right) f_y \quad (2.123)$$

and a voltage V_x is given by

$$V_x = \frac{-d_{11} f_y}{\epsilon_d l_z} \quad (2.124)$$

Deformation modes and multimorphs

Piezoelectric sensors can produce outputs in the form of charge or voltage with force, acceleration, velocity, as (displacement) inputs and then occurs 'deformation' (in the crystals). This deformation is of different types depending on the application of inputs in it. Accordingly, a number of modes are listed. In the preceding subsection, it was the thickness that changed, and accordingly the mode is named 'thickness expander mode' (TEM). The others of consequence are shown in Fig. 2.50. Other modes are length expander mode (LEM), thickness shear mode (TSM), face shear mode (FSM) and volume expander mode (VEM).

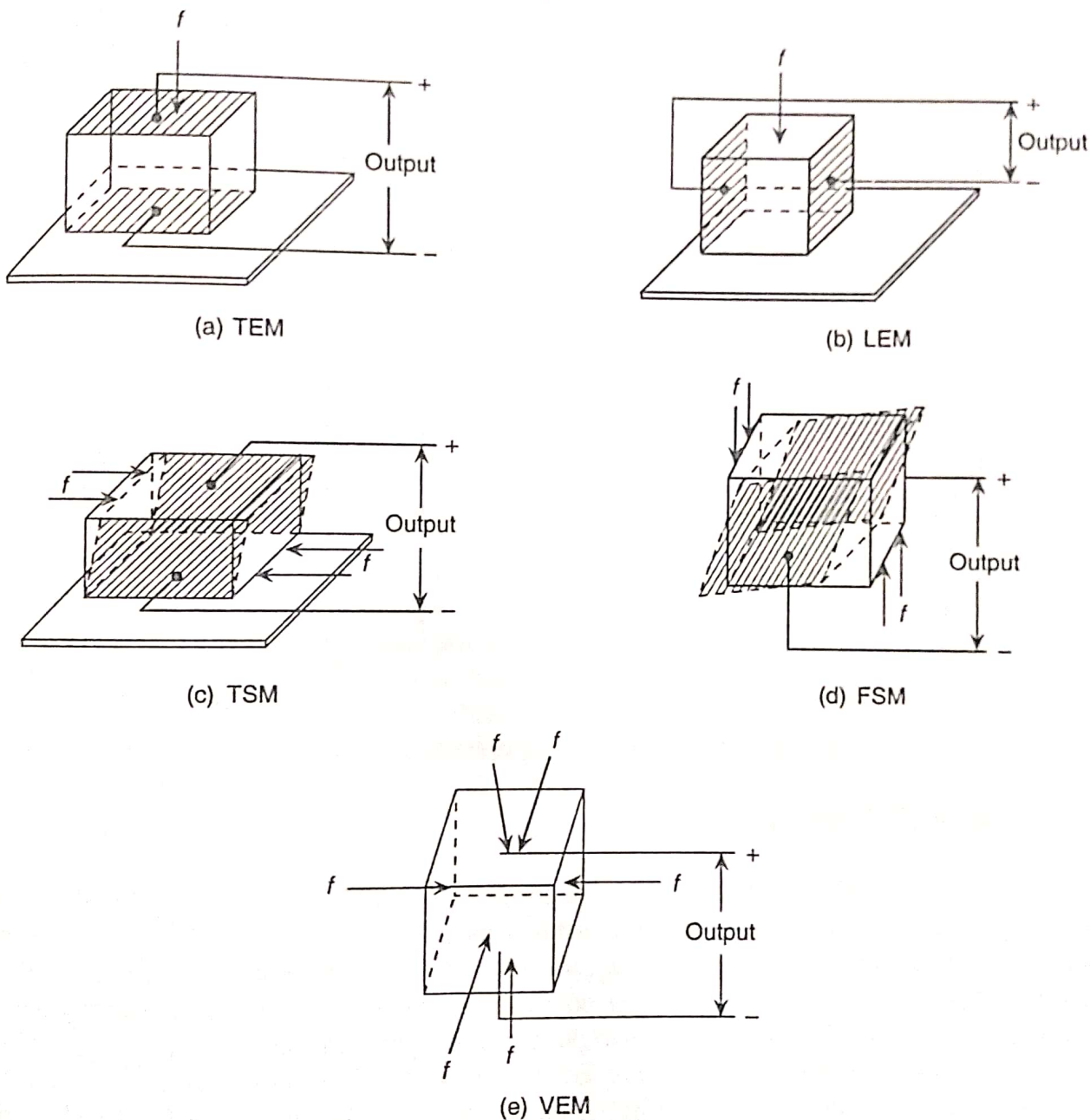


Fig. 2.50 Representation of different deformation modes: (a) thickness expander mode, (b) length expander mode, (c) thickness shear mode, (d) force shear mode, and (e) volume expander mode.

Instead of a single element sensor, it is possible to cement together two such elements as in a sandwich to obtain larger (ideally double) output. Such elements are often termed as 'bimorphs'. Proceeding in a similar way, multimorphs may be obtained for more than two elements. Bimorphs

may be obtained by series sandwiching or by parallel arrangement. Figure 2.51(a) and (b) show the two cases. In these cases, the polarization of the two plates with respect to each other, is different so that the series or parallel arrangement may be achieved. Typical bimorph cantilevers for bending (strain) and torque are shown in Figs. 2.52(a) and (b) respectively.

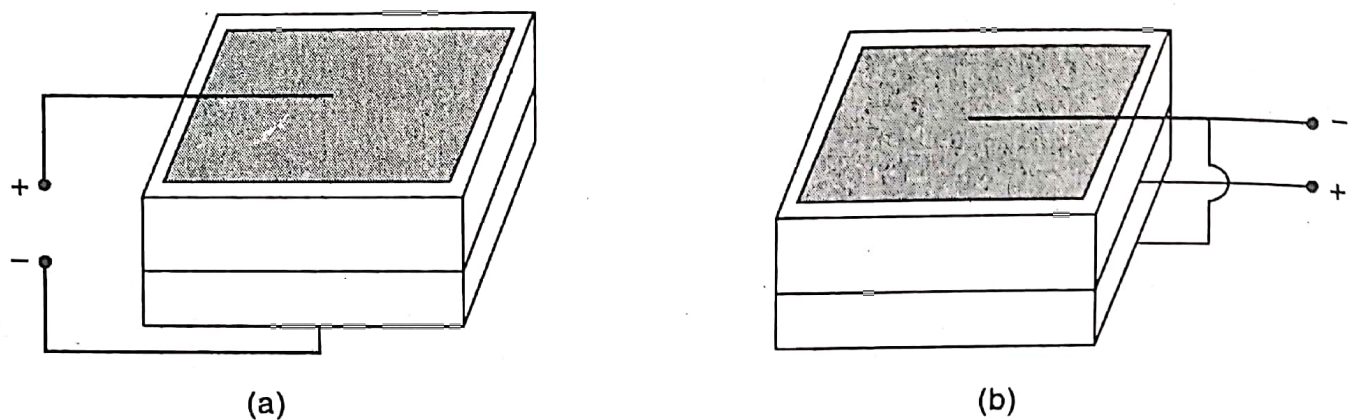


Fig. 2.51 Multimorphs: (a) series, (b) parallel.

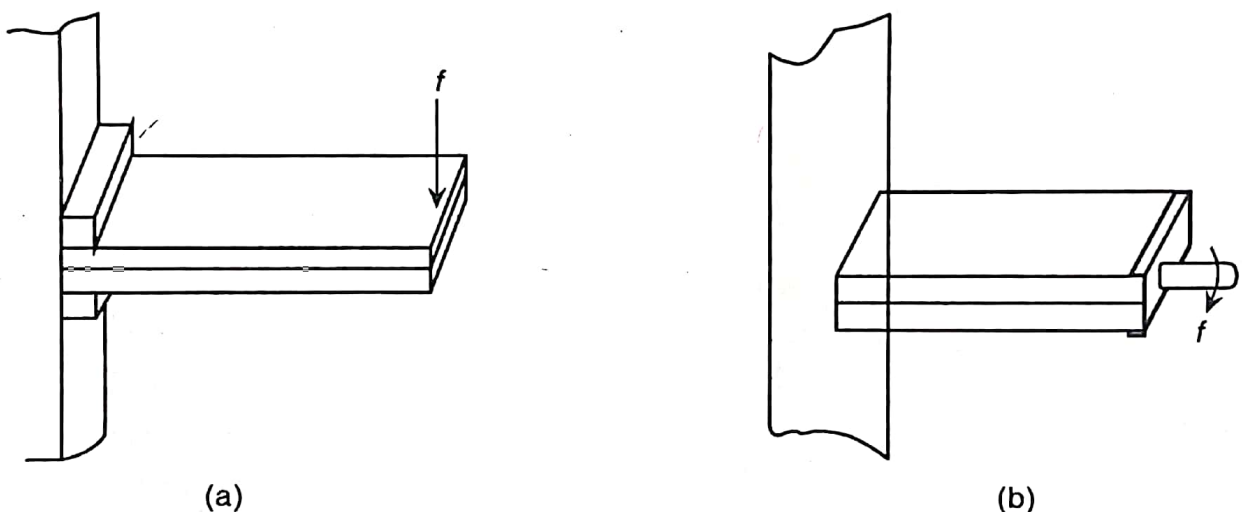


Fig. 2.52 Multimorphs applied in (a) bending, (b) torque.

2.7 ULTRASONIC SENSORS

Piezoelectric effect of certain crystalline materials has been successfully utilized in ultrasound production and sensing. This is described in detail in Section 2.5.6. Basically, it is the converse piezo-effect, that is, when an electrical field is applied to the crystal it changes its shape. This property is utilized in generating acoustic or ultrasound wave. It is to be noted that for

transmitting the wave through a medium, it is necessary that an appropriate interfacing is provided. Special types of grease are available for the purpose. Good contact is established by this interfacing.

Of the synthetic piezoelectric crystals, barium titanate (BaTiO_3) stands out as the major material which, however, requires prior polarization. It consists of randomly oriented tiny piezoelectric crystallites which are properly oriented mostly by DC polling field of several thousand volts per cm, and the material is cooled through Curie temperature. A strong piezoelectric effect has been observed in compounds such as $\text{PbZrO}_3-\text{PbTiO}_3$ called PZT materials (Section 2.5.7). This also has perovskite structure like BaTiO_3 (shown in Fig. 2.46).

Piezoelectric transducers can generate continuous wave ultrasound or pulsed ultrasound—latter being used in SONAR or other similar systems. Ultrasonic piezocrystals operate in the range of 0.5–10 MHz. They are directly attached to the transmitting medium or are separated by a small distance which is filled with coupling materials of suitable acoustic properties. Typical couplants at low temperatures are water, grease, and petrojelly and for higher temperatures special polymer couplants may be used.

For continuous wave operation, the sensor is energized by a tuned oscillator while for pulsed application ‘relaxation’ oscillators are used to charge a capacitor which is discharged across the sensor.

Analytical models describing the interactions of electrical and mechanical phenomena in piezoelectric media have been proposed but found to be inadequate for the design of piezoelectric transducers with realistic geometries and parameters of the material. Numerical solutions in three dimensions of the fundamental equations of the system, coupling the electrical and mechanical phenomena in the piezo element, are found to be necessary for the purpose. A finite element scheme is often adopted because of its inherent flexibility in handling arbitrary device geometries and anisotropies in the materials. Besides, one has to take account of the interactions of the transducer with the ambient media solutions to the wave equations which govern the propagation of acoustic waves in the ambient media flourish.

REVIEW QUESTIONS

- (a) How is the output of a potentiometric sensor affected due to shorting of windings by jockey?

For a 100 turn potentiometer, if once the 50th wire is only contacted while at the next instant, 50th and the 51st wires are shorted by the jockey, what would be the percent loss in resolution in the second case if the supply voltage is 10 V?

[Hint: Actual resolution in percentage is

$$\begin{aligned}
 100 \times \frac{\Delta V - \Delta V_k}{\Delta V} &= \{1 - nk[1/(n-1) - 1/n]\}100 \\
 &= \{1 - 100 \times 50[1/99 - 1/100]\}100 \\
 &= 49.49\%
 \end{aligned}$$

- (b) What are the different principles or schemes adopted to eliminate or at least reduce this effect? Explain with diagrams.